Electrochemical Intercalation of Potassium into Graphite

Jin Zhao, Xiaoxi Zou, Yujie Zhu, Yunhua Xu, and Chunsheng Wang*

Exceptional cycling performance of graphite anode in K-ion batteries is demonstrated with a reversible capacity of 246 mAh g^{-1} and 89% retention of the initial capacity after 200 cycles. Although the graphite anode experiences huge volume change and worse kinetics during K intercalation/deintercalation, the cycling stability delivered in K-ion batteries is comparable to that of Li-ion batteries using the same graphite anode. The combination of excellent electrochemical performance, the abundance and wide availability of K in earth's crust, and the well-developed technology of the graphite anode make the K-ion battery very attractive for offering a low cost battery chemistry for large-scale energy storage applications.

1. Introduction

As dominant power sources of portable electronics, lithium-ion battery has been considered as a potential technology for electric vehicles, renewable energy storage, and smart grids. Considering the vast implementation of lithium-ion batteries at large scale and limited resources of lithium in earth crust, the cost of lithium-ion batteries may soar up in the foreseeable future, thus creating a major barrier for the wide deployment of lithium-ion batteries.

As an alternative to lithium-ion batteries, sodium-ion[1–5] and potassium-ion[6–10] batteries have been undergoing a resurgence of interests due to the abundance and nontoxicity of sodium and potassium, which offer promises for cost-effective and environment friendly battery technology. Recently, significant advance in electrode materials for Na-ion batteries has been achieved. High performance cathodes, including metal oxides,[11–14] phosphates,[15–18] hexacyanometalates,[19–21] sulfur,[22,23] metal sulfides,[24,25] and organic materials,[26–28] have been reported, and porous carbonaceous materials and metallic Sb and Sn anodes also show high capacity and long cycling stability.[29–34] In contrast to Li-ion and Na-ion batteries, very few studies on K-ion batteries have been reported.[6–10]

Graphite, a standard anode in commercial Li-ion batteries through electrochemical formation of graphite intercalation compounds (GICs), has low capacity with fast capacity decay to potassium,[7] and is electrochemically inactive to sodium ions.[35,36] GICs have been extensively studied in last century because of its appealing physical, chemical, and electronic characteristics in superconductors, catalysts, and Li-ion batteries.[35] GICs are produced by inserting different chemical species into carbon layers of graphite without destroying the layered structure of the host graphite. Many metal atoms have been reported to be able to intercalate into graphite to form layered structures, particularly lithium GICs have been successfully employed in batteries. Although potassium GICs have been thoroughly studied in structures and chemical/physical properties last century,[35] little attention has been given to its application in batteries. Actually, stage phenomena of ternary potassium-dimethyl sulfoxide-GICs have been studied by electrochemically intercalating solvated potassium into graphite to different intercalation levels.[37–39] The electrochemically reversible intercalation/deintercalation of alkali metal in graphite has been observed during the study of electrochromic effects of GICs as early as 1970s.[40,41] Recently, the electrochemically reversible intercalation of potassium into graphite was also proved in molten salt of KF at 1163 K, in which the electrochemical reversibility was evidenced by cyclic voltammetric measurement and X-ray diffraction (XRD) analysis.[42,43] Unfortunately, the high temperature, the instability of the resulting K-GICs in molten KF, and severe structure damage of graphite during the insertion/deinsertion processes make this system unsuitable for energy storage. In 1997, KC_8, a fully intercalated K-GIC, prepared by two-zone vapor transport method was used as anode in Li-ion batteries and the successful extraction of potassium was identified by recovered graphite structure after releasing potassium.[44] Very recently, Ji group reported room temperature electrochemical performance of potassium GICs using graphite, where the electrochemically reversible formation of stage phases of potassium GICs was confirmed by ex situ XRD measurement.[7] However, mechanism behind the poor cycling stability (capacity loss of 0.98% per cycle) and slow kinetics of electrochemical intercalation of K into graphite needs to be explored.

J. Zhao, Prof. Y. H. Xu
School of Material Science
Tianjin University
Tianjin 300072, China
E-mail: yunhua.xu@tju.edu.cn
Prof. Y. H. Xu
Collaborative Innovation Center of
Chemical Science and Engineering (Tianjin)
Tianjin 300072, China
X. Zou
School of Materials Science and Engineering
Wuhan Institute of Technology
Wuhan 430073, China
Prof. Y. J. Zhu
School of Chemistry and Environment
Beihang University
Beijing 100191, China
Prof. C. S. Wang
Department of Chemical and Biomolecular Engineering
University of Maryland
College Park, MD 20742, USA

DOI: 10.1002/adfm.201602248

In this work, the electrochemical performance and kinetics of graphite anode in K-ion batteries was systematically studied and compared with those of Li-ion batteries using the same graphite anode. A reversible capacity of 246 mAh g^{-1} was achieved and remained 89% of the initial capacity after 200 cycles in K-ion batteries, which is better than those of graphene, hollow carbon spheres, and nitrogen-doped carbon anodes, and comparable with that of hard carbon anodes in Na-ion batteries (Table S1 in Supporting Information). The cycling stability of graphite anode in K-ion batteries is comparable to that in Li-ion batteries, and the capacity decay rate (0.053% per cycle) is more than one order of magnitude less than the reported value (0.98% per cycle).[7] Most importantly, the use of graphite anodes in K-ion batteries can adopt the well-developed anode technology in Li-ion batteries. Considering the abundance of K in earth crust (the seventh abundant element), which is next to Na (the sixth abundant element), and similar behaviors of K-ion batteries to those Li-ion batteries, it is much more attractive to provide a high performance and low-cost battery technology instead of Na and Li for emerging large-scale application of energy storage.

2. Results and Discussion

The electrochemical intercalation performance of K into graphite was investigated using high purity and well-crystalline graphite (TIMCAL TIMREX KS4) as revealed by XRD data (Figure S1, Supporting Information). The scanning electron microscopy (SEM) images show that KS4 has a flake shape (Figure S2, Supporting Information). The graphite electrode was prepared by casting a slurry consisting of 90% graphite and 10% Na-alginate binder onto Cu foils. K-ion coin batteries were assembled in glove box using electrolyte of 1 M KPF_6 in ethylene carbonate: propylene carbonate (EC:PC, 1:1 by volume), EC:diethyl carbonate (DEC) or EC:dimethyl carbonate (DMC) and counter and reference electrodes of potassium metal. For comparison, the same graphite electrodes were also used to assemble Li-ion batteries but using 1 M $LiPF_6$ in EC:PC (1:1 by volume) as electrolyte and lithium foil as counter and reference electrodes. All batteries were constructed and tested in the same conditions.

The ion intercalation/deintercalation behaviors of graphite in K-ion and Li-ion batteries in EC:PC electrolytes were characterized using cyclic voltammogram (CV) at a scan rate of 0.01 mV s^{-1} between 0 and 1.0 V (**Figure 1**). Three well-resolved Li intercalation/deintercalation redox couples at 0.05/0.12, 0.09/0.16, and 0.19/0.23 V can be observed for the KS4 graphite anodes in Li-ion batteries (Figure 1b), corresponding to the well-known stage phase transformation processes between dilute Stages 1 and 4, Stages 2 and 3, and Stages 2 and 1, respectively.[45,46] The CV curves are in good agreement with standard CV scan of graphite reported for Li ion intercalation.[45,46] Therefore, KS4 graphite can be reliably used to characterize the K ion intercalation behavior. In contrast to Li intercalation/deintercalation, K intercalation/deintercalation shows one

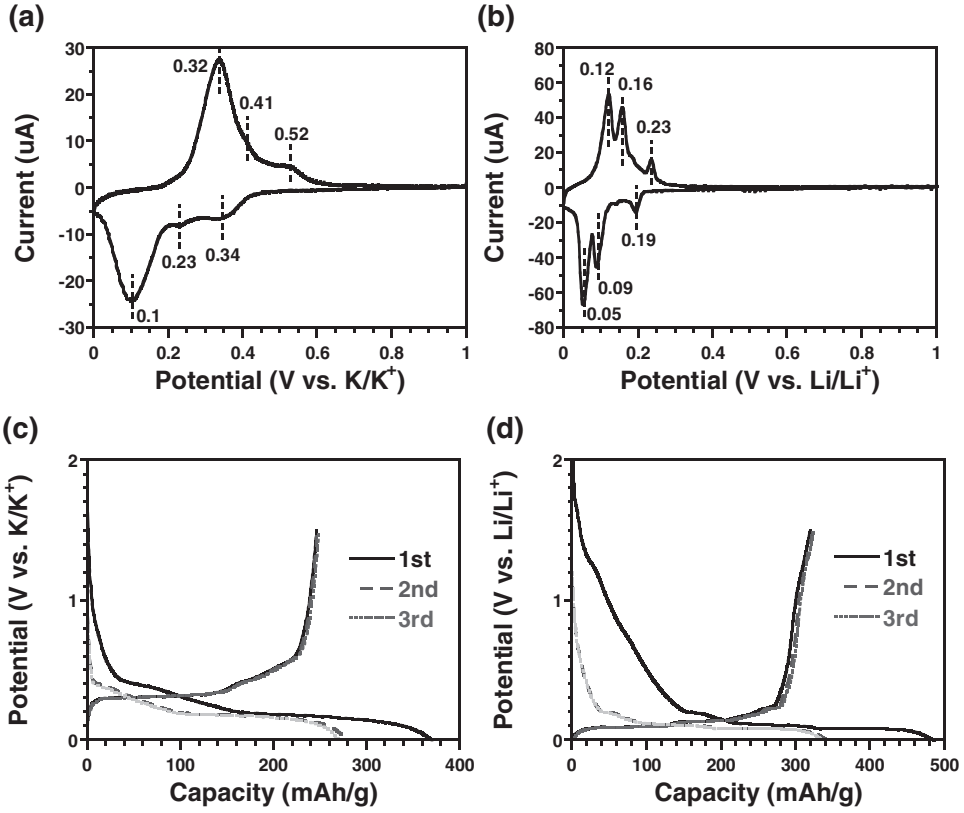

Figure 1. a,b) CV curves and c,d) charge/discharge voltage profiles of graphite in a,c) K-ion and b,d) Li-ion batteries with the same graphite anodes in EC:PC electolytes.

distinct redox couple at 0.1/0.32 V with two shoulder couples at 0.23/0.41 and 0.34/0.52 V, respectively (Figure 1a). The strong cathodic peak is assigned to the transformation to intercalation compound of Stage 1, while the two cathodic shoulders account for the phase transition to Stage 2 and Stage 3, respectively.[7] The well-reversible anodic and cathodic processes demonstrate the high reversibility of K intercalation/deintercalation in graphite. However, a much larger polarization between anodic/cathodic peaks (0.22 V) was observed in K-ion batteries compared to that of Li-ion batteries (0.07 V) (Figure 1b), revealing worse intercalation kinetics of K into graphite since identical graphite was used for Li and K intercalation/deintercalation. This is caused by the larger ionic radius of K ions than that of Li ions, as observed in Sn anodes versus Li and Na.[32] There is a big decrease in cathodic peak current from the first cycle to the following cycles (Figure S3, Supporting Information). This is attributed to the decomposition of electrolyte to form solid-electrolyte interphase (SEI) film. The similar anodic peak intensity in the first five cycles indicates a stable cycling performance of graphite anodes in K-ion batteries.

The ion intercalation/deintercalation behaviors of K and Li in graphite were also compared during galvanostatic charge/discharge at 20 mA g^{-1} between 0 and 1.5 V (Figure 1c,d). Different from Li ion intercalation, where three successive voltage plateaus due to stage transformation are clearly presented (Figure 1d), only one discharge (potasiation) voltage plateau at 0.17 V and a slope at 0.4–0.2 V were observed for K ion intercalation (Figure 1c). The voltage slope is attributed to the intercalation process to form Stage 2 phase of KC_{24}, while the plateau is a coexistence regime of Stage 1 (KC_8) and Stage 2 (KC_{24}), i.e., phase transition region. Upon charge (depotasiation), the phase transformation plateau and slope shift up to 0.31 V and 0.35–0.6 V, respectively. As observed in CV curves (Figure 1a,b), the larger voltage hysteresis of 0.14 V between charge and discharge for K than that of Li (0.015 V) is induced by the slow diffusion kinetics of K ions in graphite due to its larger ionic radius.[18,32]

Although the standard electrode potential of K (–2.93 V) is higher than that of Li (–3.04 V), a higher intercalation potential of graphite for K-ion intercalation than that for Li-ion intercalation demonstrates that K insertion into graphite is more favorable than Li insertion. Computational studies on the intercalation energetics of Li and K into graphite reveal that the formation of LiC_6 and KC_8 is an exothermic process with formation enthalpy of –16.4 and –27.5 kJ mol^{-1}, respectively.[47] The larger energy change during the intercalation process may account for the easier intercalation of K into graphite than Li.

The higher intercalation potentials for K offer additional safety merits by avoiding/reducing plating or dendrite formation on the graphite surface at very low potential observed in Li-ion batteries.[48,49] A capacity of 370 mAh g^{-1} was delivered in the first potasiation and 246 mAh g^{-1} in the first depotasiation, giving to a Coulombic efficiency of 66.5%, which is similar to that of Li-ion batteries (65.8%) (Figure 1c,d). The depotasiation capacity is close to the theoretical capacity of 279 mAh g^{-1} for fully intercalated KC_8. The irreversible capacity in the first cycle is assigned to the formation of SEI films due to the decomposition of electrolyte. The barely changed voltage profiles after the first K intercalation clearly indicate good reversibility and stability of graphite in K-ion batteries (Figure 1c).

The phase nature of graphite before K intercalation, after full K intercalation and after full deintercalation, was investigated using XRD diffraction and Raman spectroscopy (**Figure 2**). Pristine graphite shows typical graphite characteristics of a

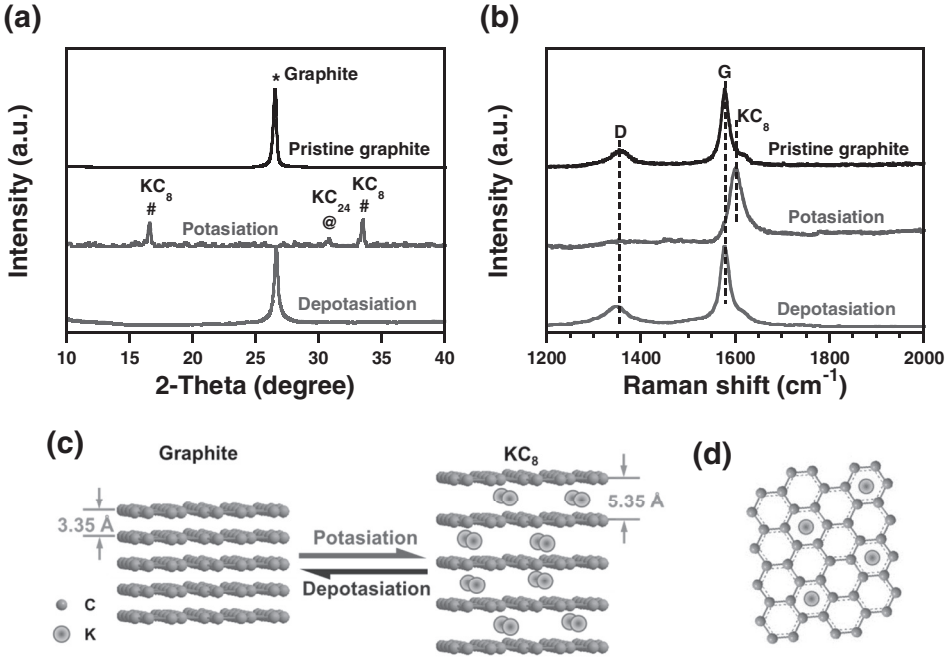

Figure 2. a) XRD pattern and b) Raman spectra of fresh graphite anodes and at potasiation and depatasiation states. c) Schematic illustration of potasiation/depotasiation processes of graphite, which shows the interlayer distance expanded from 3.35 to 5.35 Å upon the intercalation of K, and d) schematic diagram of in-plane pattern for KC_8.

sharp peak at the two-theta angle of 26.5°. At full potasiation state, the graphite peak vanished, characteristic peaks of KC_8 at 16.2 and 33.5° appear, indicating the formation of fully intercalated potassium GIC. The XRD pattern is consistent with the XRD measurements of KC_8 GICs prepared by chemical methods.[35,50,51] The formation of KC_8 was also evidenced by the color change from black of pristine graphite to brown color of the potasiated graphite revealed by the photo pictures in Figure S4 (Supporting Information).[40,41] A small peak at 30.6° may be attributed to the residue of Stage 2 of K-GIC (KC_{24}).[50] After depotasiation, the graphite peak was fully recovered, revealing the complete deintercalation of K from graphite interlayers and restacking of graphene layers. The changes in interlayer distance of fresh graphite, after K ion intercalation and after deintercalation, were calculated using XRD peaks. The interlayer distance of fresh graphite is 3.35 Å, and increases to 5.35 Å after K intercalation (Figure 2c,d),[35,51] which is much larger than that of lithiated graphite of LiC_6 (3.706 Å, Figure S5, Supporting Information). The corresponding volume expansion of graphite due to change in interlayer distance is estimated to be 59.7% at full K intercalation, which is almost six times larger than that of Li intercalation (10.7%). Unlike alloy and conversion electrode materials in which large volume expansion significantly diminish cycling stability and structure reversibility,[18,32] the large volume change of graphite during potasiation/depotasiation can completely recover the original layer structure of graphite. This unique behavior may provide a new direction in designing and developing electrode materials.

The reversible intercalation of K into graphite is also revealed by Raman spectra of the fresh graphite electrode and those at fully intercalated and deintercalated states (Figure 2b). Typical peaks at 1350 cm^{-1} (D-band) and 1580 cm^{-1} (G-band) for the fresh electrodes were observed, but disappeared in fully potasiated graphite, instead a new peak at 1600 cm^{-1} assigned to KC_8 is present, indicating the successful intercalation of K into graphite.[50] The reversibility was verified by the recovery of graphite peaks after depotasiation (Figure 2b).

The cyclability of the KS4 graphite in K-ion batteries was examined at a constant charge/discharge current density of 20 mA g^{-1} between 0–1.5 V (**Figure 3**a). Different from previous report,[7] exceptional cycling stability was demonstrated for K-ion batteries with capacity retention of 220 mAh g^{-1} after 200 cycles and capacity decay rate of 0.053% per cycle, (Figure 3a), which is one order of magnitude less than the capacity decay (0.98% per cycle) reported.[7] A high Coulombic efficiency of 98% was obtained after initial ten cycles (Figure 3b). The cycling stability of KS4 for K intercalation/deintercalation is comparable to that for Li intercalation/deintercalation (Figure S6, Supporting Information) although kinetics of graphite for K intercalation is worse than that for Li.

The layered structure of graphene sheets that are bonded together by van der Waals' force is physically, chemically, and electrochemically stable during ion intercalation/deintercalation, assuring a stable carbon host. Upon metal ion intercalation, interlayer distance of graphene sheets expands along with c-axis, leading to volume expansion, but the size of in-plane structure of graphene sheets is almost unchanged. During deintercalation, graphene sheets restack back to the original layered structure of graphite under van der Waals' interaction force as evidenced by the XRD and Raman analysis in Figure 2 for K-ion batteries and previous reports for Li-ion batteries.[46] Therefore, although K ions are much bigger than Li ions, good reversibility of electrochemical intercalation of both Li and K into graphite can be achieved. The high structure reversibility of graphite has also been reported on the co-intercalation of solvent/Na ions with large volume change.[52]

The effects of electrolytes on the electrochemical performance of graphite in K-ion batteries were investigated in three kinds of electrolytes of 1 M KPF_6 in EC:PC, EC:DEC and EC:DMC, respectively. As illustrated by the charge/discharge voltage profiles in Figure 1c and Figure S7 (Supporting Information), similar reversible capacity of about 240 mAh g^{-1} and similar charge/discharge voltage profiles in the first three cycles were observed, indicating successful intercalation of K ions into graphite for the three electrolytes. Significant difference, however, appears in Coulombic efficiency and cycling stability for the three electrolytes (Figure 3). In the first cycle, Coulombic efficiencies of 47.0% and 42.7% were obtained in KPF_6:EC:DEC and KPF_6:EC:DMC electrolytes, respectively, much lower than 66.5% in KPF_6:EC:PC electrolyte. The large amount of irreversible capacity in the former two cases may be caused by more severe decomposition of DEC and DMC that are not stable at low voltage.[53,54] The Coulombic efficiency quickly increases to 95% after ten cycles in the case of EC:PC

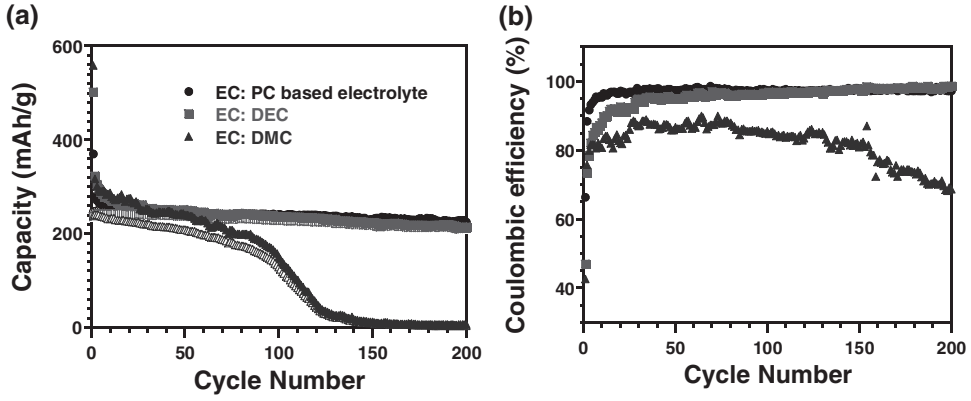

Figure 3. Comparasion of a) cycling performance and b) Coulombic efficiency of graphite anodes in K-ion batteries in different electrolytes of KPF_6 in EC:PC, EC:DEC, and EC:DMC.

electrolyte, while it takes more than 30 cycles in KPF_6:EC:DEC electrolyte, implying that more DEC is consumed to form a stable SEI layer. The Coulombic efficiency of KPF_6:EC:DMC electrolyte maintains a low efficiency of below 90% for all test cycles and quickly decreases after 70 cycles, suggesting that no stable SEI film formed and severe and continuous decomposition of DMC occurred. The cycling stability presents the same trend as observed in Coulombic efficiency. A capacity retention of 200 mAh g^{-1} after 200 cycles was observed in EC:DEC electrolyte, lower than 220 mAh g^{-1} in EC:PC electrolyte, indicating a worse stability than in EC:PC electrolyte. The EC:DMC electrolyte is the worst one, which presents a continuous capacity decrease and failed after 140 cycles. Clearly, the worse performance in EC:DMC electrolyte is associated with the poor electrochemical stability of DMC upon reduction.[53,54] The EC:PC based electrolyte is also found to be the best electrolyte for Na-ion batteries in terms of reversible capacity, Coulombic efficiency, and cycle life due to more stable SEI formed.[53,54] Therefore, although optimization of electrolytes is still needed for further enhancing the cycling stability of graphite anodes in K-ion batteries, the complete reversibility of K intercalation into graphite provides an opportunity to develop a long cycle life of K-ion batteries with graphite electrode.

The role of binders in electrochemical performance of graphite in K-ion batteries was also examined by testing polyvinylidene fluoride (PVDF) and Na alginate at the same conditions. As revealed by the charge/discharge voltage profiles in Figure S8a (Supporting Information), PVDF shows a much lower Coulombic efficiency of 44.5% than Na alginate (66.5%). The enhancement in Coulombic efficiency by using Na alginate binder may be attributed to its better coatability than PVDF, which enables more uniform coating layer that would reduce the formation of SEI film.[55] A graphite anode using PVDF binder shows gradual degradation in capacity (Figure S8b, Supporting Information). The results are consistent with previous reports on graphite in K-ion batteries using PVDF.[7] Therefore, in addition to electrolytes, binders also play an important role in optimizing the electrochemical performance of K-ion batteries.

The reaction kinetics of K intercalation into graphite were also investigated using galvanostatic intermittent titration technique (GITT) and electrochemical impedance spectroscopy (EIS). GITT measurement was performed by applying a series of current pulses at 20 mA g^{-1} for 1 h followed by a 10 h relaxation process (**Figure 4** and Figure S9, Supporting Information). The open-circuit-voltage at the end of the long-time relaxation is considered to be quasithermodynamically equilibrium potential. The quasithermodynamically equilibrium potential shows one slope line and one long plateau at 0.23 V (Figure 4a). A potential hysteresis of 15 mV between K intercalation and deintercalation (Figure 4a) was observed due to large strain/stress during K intercalation/deintercalation processes, which is much larger than that of Li intercalation/deintercalation (3 mV, Figure S10, Supporting Information), but is still smaller than that of alloy anodes such as Si and Sn.[32] Potassium also undergoes worse kinetics than Li as revealed by GITT and EIS measurement results presented below. As a result, poor rate capability was observed for graphite anodes in K-ion batteries. The rate performance was tested at current densities from 20 to 500 mA g^{-1} (Figure S11, Supporting Information). The

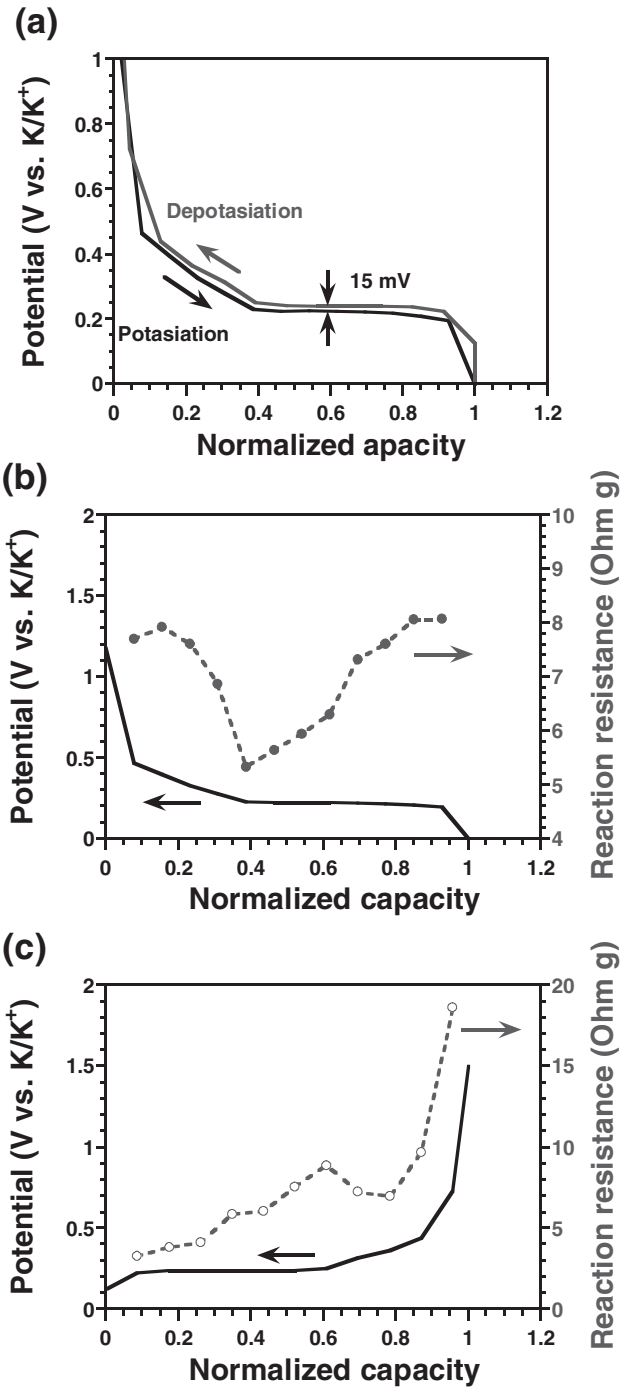

Figure 4. a) Quasi-thermodynamically equilibrium potential profiles and reaction resistance during b) potasiation and c) depotasiation processes of graphite in K-ion batteries in EC:PC electrolyte. For comparison, the capacity was normalized to the maxium potasiation/depotasiation capacity values.

K-ion batteries suffer a fast capacity roll-off when the current density increased and failed to deliver capacity at 500 mA g^{-1}. For future application, the kinetics needs to be improved to enhance the rate capability.

Reaction resistance, calculated by dividing the overpotential by the pulse current density, was used to probe the reaction

kinetics. Figure 4b, c presents the reaction resistance at different K intercalation/deintercalation levels and the corresponding quasi-equilibrium potentials. In the voltage slope region from 0.4 to 0.23 V, the reaction resistance increases and then decreases from 7.7 Ohm g to a minimum value of 5.3 Ohm g. In the following voltage plateau of phase transformation region, it gradually increases to the original level. The reduction in reaction resistance in the slope area can be explained by the improved conductivity of intercalated graphite caused by both potassium intercalation and volume expansion. Alkali metal GICs have been reported to have much higher conductivity even at a low intercalation level,[35] and the volume expansion can also considerably improve the electric contact between graphite particles, thus enhancing contact conductivity.[18,32,45] The increase in reaction resistance during the phase transformation is owed to accumulated strain/stress and gradual increase of the K ion diffusion length,[45,56] which can be partially relaxed in the solid solution region, as demonstrated by the decreased resistance in the slope region.[45]

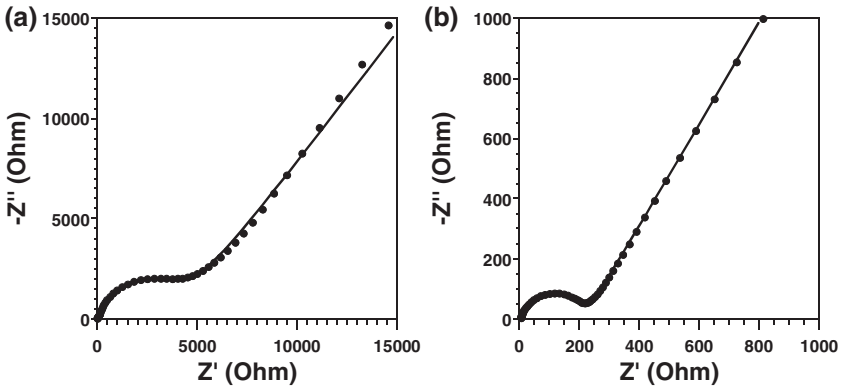

Figure 5. Nyquist plots of graphite anodes in EC:PC electrolytes obtained in EIS test in a) K-ion and b) Li-ion batteries after three activation cycles. The solid lines are the fitting curves by using the equivalent circuits which are shown in Figure S9 (Supporting Information).

Similar to the K intercalation, the reaction resistance during K deintercalation also increases in the phase transformation plateau region, and then reduces in the solid solution region, following with a rapid increase again (Figure 4c). In the beginning of K deintercalation, the extraction of potassium occurred on the edge area of graphite particles and thus the short transport distance leads to a low reaction resistance. On one hand, as the phase transformation progresses, the potassium concentration polarization and diffusion length gradually increase, leading to the increase of reaction resistance. On the other hand, the reduced electric conductivity of graphite caused by the deintercalation of potassium and the insufficient electric contact between graphite particles or graphite and current collectors originated from the huge volume contraction contributes to the rising reaction resistance. Similar resistance change behaviors have been reported for graphite in Li-ion batteries where graphite experiences three reaction resistance jumps in the three successive phase transformation regions.[45,57]

The intercalation kinetics of graphite at full deintercalation stage for K and Li after three activation cycles was compared using EIS in the frequency range of 10 MHz–0.01 Hz at 10 mV amplitude. The Nyquist plots of graphite versus K and Li were shown in **Figure 5**a and b, respectively. A depressed semicircle at high frequency and a straight line at low frequency were presented. The high-frequency depressed semicircle presents the total resistances of contact and charge transfer, while the low-frequency slope line accounts for ion diffusion and phase transformation in graphite. The high-frequency depressed semicircle of graphite in K-ion batteries is much larger than that of Li-ion batteries, revealing larger interface resistance for K than Li. In addition, the ion diffusion and phase transformation resistance for K intercalation into graphite is also larger than that for Li intercalation into graphite.

The impedance data were further fitted with equivalent circuits shown in Figure 5 and Figure S12 (Supporting Information), where R_s represents the electrolyte resistance, R_{ct} and R_f correspond to the charge transfer resistance and the contact resistance related to SEI films, respectively. The resistance values are summarized in Table S2 (Supporting Information). It was seen that the electrolyte resistance in K-ion batteries is smaller than that in Li-ion batteries, which is attributed to the larger transport number and higher mobility of potassium electrolyte than those of lithium electrolyte.[10] The charge transfer resistance, however, is more than one order of magnitude larger for K-ion batteries than Li-ion batteries. This should be associated with the larger ionic radius of K ions than that of Li ions. The total resistance including electrolyte, charge transfer, and contact resistances in K-ion batteries is much larger than that in Li-ion batteries, which is consistent with the observations in GITT measurement.

3. Conclusion

In summary, electrochemical performance, structure change, and intercalation kinetics of graphite anode in K-ion batteries were investigated and compared to those of the same graphite in Li-ion batteries using CV, charge/discharge voltage profiles, XRD, Raman, GITT and EIS measurement. The XRD and GITT results revealed that although the graphite anode experienced larger volume change (≈60%) and worse kinetics during K intercalation/deintercalation, a comparable cycling stability was achieved for K-ion batteries to that of Li-ion batteries. It was found that electrolytes and binders play important roles in determining the electrochemical performance of graphite anodes in K-ion batteries. EC:PC based electrolyte and Na alginate binder demonstrated superior cycling performance to others, such as higher Coulombic efficiency and better cycling stability. The results may inspire new ideas in design and development of high performance electrode materials and new battery chemistry. A higher reaction potential was observed in K-ion batteries, which reduces safety hazards caused by plating/striping of K on the surface of graphite at low voltage. The excellent electrochemical performance, coupled with the abundance and wide availability of K in earth crust and well-developed technology of graphite anode, makes K-ion batteries

appealing in offering a lower cost and safer battery chemistry for stationary applications.

4. Experimental Section

Material Characterizations: SEM images were taken by Hitachi SU-70 analytical ultra-high resolution SEM (Japan). XRD pattern was recorded by Bruker Smart1000 (Bruker AXS Inc., USA) using CuKα radiation on pristine and charged/discharged samples. Raman measurements were performed on a Horiba Jobin Yvon Labram Aramis using a 532 nm diode-pumped solid-state laser, attenuated to give ≈900 μW power at the sample surface on fresh and intercalated/deintercalated graphite anodes. The intercalated/deintercalated samples were obtained by disassembling batteries at the corresponding states inside argon-filled glove box and sealed with Capton tape before moving out of glove box.

Electrochemical Measurements: The graphite electrode was prepared by mixing graphite (90%) and 10% Na-alginate or PVDF binder to form slurry and cast on Cu foils using a doctor blade and dried in a vacuum at 100 °C overnight. K-ion batteries were assembled with electrolytes of 1 M KPF_6 in EC:PC (1:1 by volume), EC:DEC (1:1 by volume), and EC:DMC (1:1 by volume) and counter and reference electrodes of potassium metal. Li-ion batteries were assembled using the same graphite electrodes but using electrolyte of 1 M $LiPF_6$ in EC:PC (1:1 by volume) and counter and reference electrodes of lithium metal. Separator of Celgard3501 (Celgard, LLC Corp., USA) was used in the battery assembly.

Electrochemical performance was tested using Arbin battery test station (BT2000, Arbin Instruments, USA). Cyclic voltammogram at a scan rate of 0.01 mV s^{-1} between 0–1.0 V, GITT data, and EIS spectra of graphite anodes were recorded using Solatron 1260/1287 Electrochemical Interface (Solatron Metrology, UK). GITT measurement was performed by applying a series of current pulses at 20 mA g^{-1} for 1.0 h followed by a 10 h relaxation process. EIS data were measured on fully charged state after three cycles in the frequency range of 10 MHz to 0.01 Hz at 10 mV amplitude.

Supporting Information

Supporting Information is available from the Wiley Online Library or from the author.

Acknowledgements

The authors acknowledge the financial support from the Thousand Talents Plan for Young Professionals of China and the Outstanding Young Scholar Program of Tianjin University. The authors thank Tao Gao and Ying Liu for their help with the analysis and fitting of EIS data.

Received: May 6, 2016
Revised: July 11, 2016
Published online: September 26, 2016

[1] N. Yabuuchi, K. Kubota, M. Dahbi, S. Komaba, *Chem. Rev.* **2014**, *114*, 11636.
[2] S. W. Kim, D. H. Seo, X. H. Ma, G. Ceder, K. Kang, *Adv. Energy Mater.* **2012**, *2*, 710.
[3] X. D. Xiang, K. Zhang, J. Chen, *Adv. Mater.* **2015**, *27*, 5343.
[4] V. palomares, P. Serras, I. Villaluenga, K. B. Hueso, J. Carretero-González, T. Rojo, *Energy Environ. Sci.* **2012**, *5*, 5884.
[5] H. Pan, Y. Hu, L. Chen, *Energy Environ Sci.* **2013**, *6*, 2338.
[6] Y. Liu, F. Fan, J. Wang, Y. Liu, H. Chen, K. L. Jungjohann, Y. Xu, Y. Zhu, D. Bigio, T. Zhu, C. Wang, *Nano Lett.* **2014**, *14*, 3445.
[7] Z. Jian, W. Luo, X. Ji, *J. Am. Chem. Soc.* **2015**, *137*, 11566.
[8] Z. Jian, Z. Xing, C. Bommier, Z. Li, X. Ji, *Adv. Energy Mater.* **2015**, *5*, 1501874.
[9] W. Luo, J. Wan, B. Ozdemir, W. Bao, Y. Chen, J. Dai, H. Lin, Y. Xu, F. Gu, V. Barone, L. Hu, *Nano Lett.* **2015**, *15*, 7671.
[10] S. Komaba, T. Hasegawa, M. Dahbi, K. Kubota, *Electrochem. Commun.* **2015**, *60*, 172.
[11] Y. Wang, J. Liu, B. Lee, R. Qiao, Z. Yang, S. Xu, X. Yu, L. Gu, Y. Hu, W. Yang, K. Kang, H. Li, X. Yang, L. Chen, X. Huang, *Nat. Commun.* **2015**, *6*, 6401.
[12] N. Yabuuchi, M. Kajiyama, J. Iwatate, H. Nishikawa, S. Hitomi, R. Okuyama, R. Usui, Y. Yamada, S. Komaba, *Nat. Mater.* **2012**, *11*, 512.
[13] J. Y. Hwang, S. M. Oh, S. T. Myung, K. Y. Chung, I. Belharouak, Y. K. Sun, *Nat. Commun.* **2015**, *6*, 6865.
[14] M. Xu, Y. Niu, C. Chen, J. Song, S. Bao, C. M. Li, *RSC Adv.* **2014**, *4*, 38140.
[15] Z. Jian, W. Han, X. Lu, H. Yang, Y. Hu, J. Zhou, Z. Zhou, J. Li, W. Chen, D. Chen, L. Chen, *Adv. Energy Mater.* **2013**, *3*, 156.
[16] J. Kim, D. Seo, H. Kim, I. Park, J. Yoo, S. Jung, Y. Park, W. A. Goddard III, K. Kang, *Energy Environ. Sci.* **2015**, *8*, 540.
[17] Y. Zhou, X. Rui, W. Sun, Z. Xu, Y. Zhou, W. J. Ng, Q. Yan, E. Fong, *ACS Nano* **2015**, *9*, 4628.
[18] Y. Zhu, Y. Xu, Y. Liu, C. Luo, C. Wang, *Nanoscale* **2013**, *5*, 780.
[19] Y. You, X. Wu, Y. Yin, Y. Guo, *Energy Environ. Sci.* **2014**, *7*, 1643.
[20] L. Wang, Y. Lu, J. Liu, M. Xu, J. Cheng, D. Zhang, J. B. Goodenough, *Angew. Chem. Int. Ed.* **2013**, *52*, 1964.
[21] X. Wu, W. Deng, J. Qian, Y. Cao, X. Ai, H. Yang, *J. Mater. Chem. A* **2013**, *1*, 10130.
[22] S. Xin, Y. Yin, Y. Guo, L. Wan, *Adv. Mater.* **2014**, *26*, 1261.
[23] S. Zheng, P. Han, Z. Han, P. Li, H. Zhang, J. Yang, *Adv. Energy Mater.* **2014**, *4*, 1400226.
[24] Z. Hu, Z. Zhu, F. Cheng, K. Zhang, J. Wang, C. Chen, J. Chen, *Energy Environ. Sci.* **2015**, *8*, 1309.
[25] Y. Zhu, L. Suo, T. Gao, X. Fan, F. Han, C. Wang, *Electrochem. Commun.* **2015**, *54*, 18.
[26] H. Wang, S. Yuan, D. Ma, X. Huang, F. Meng, X. Zhang, *Adv. Energy Mater.* **2014**, *4*, 1301651.
[27] W. Luo, M. Allen, V. Raju, X. Ji, *Adv. Energy Mater.* **2014**, *4*, 1400554.
[28] C. Luo, R. Huang, R. Kevorkyants, M. Pavanello, H. He, C. Wang, *Nano Lett.* **2014**, *14*, 1596.
[29] J. Zhao, L. Zhao, K. Chihara, S. Okada, J. Yamaki, S. Matsumoto, S. Kuze, K. Nakane, *J. Power Sources* **2013**, *244*, 752.
[30] S. Komaba, W. Murata, T. Ishikawa, N. Yabuuchi, T. Ozeki, T. Nakayama, A. Ogata, K. Gotoh, K. Fujiwara, *Adv. Funct. Mater.* **2011**, *21*, 3859.
[31] Y. Zhu, X. Han, Y. Xu, Y. Liu, S. Zheng, K. Xu, L. Hu, C. Wang, *ACS Nano* **2013**, *7*, 6378.
[32] Y. Xu, Y. Zhu, Y. Liu, C. Wang, *Adv. Energy Mater.* **2013**, *3*, 128.
[33] Y. Liu, Y. Xu, Y. Zhu, J. N. Culver, C. A. Lundgren, K. Xu, C. Wang, *ACS Nano* **2013**, *7*, 3627.
[34] L. Xiao, Y. Cao, J. Xiao, W. Wang, L. Kovarik, Z. Nie, J. Liu, *Chem. Commun.* **2012**, *48*, 3321.
[35] M. S. Dresselhaus, G. Dresselhaus, *Adv. Phys.* **2002**, *51*, 1.
[36] Y. Okamoto, *J. Phys. Chem. C* **2014**, *118*, 16.
[37] J. O. Besenhard, *Carbon* **1976**, *14*, 111.
[38] J. O. Besenhard, H. Mohwald, J. J. Nickl, *Carbon* **1980**, *18*, 399.
[39] B. Marcus, P. Touzain, *J. Solid State Chem.* **1988**, *77*, 223.
[40] P. Pfluger, H. U. Künzi, H.-J. Güntherodt, *Appl. Phys. Lett.* **1979**, *35*, 771.
[41] P. Pfluger, P. Oelhafen, H. U. Künzi, R. Jeker, E. Hauser, K. P. Ackermann, M. Müller, H.-J. Güntherodt, *Physica B* **1980**, *99*, 395.

[42] D. Liu, Z. Yang, W. Li, S. Qiu, Y. Luo, *Electrochim. Acta* **2010**, *55*, 1013.
[43] D. Liu, W. Li, Z. Yang, S. Qiu, Y. Luo, *Trans. Nonferrous Met. Soc. China* **2011**, *21*, 166.
[44] R. Tossici, M. Berrettoni, M. Rosolen, R. Marassi, *J. Electrochem. Soc.* **1997**, *144*, 186.
[45] C. Wang, I. Kakwan, A. J. Appleby, F. E. Little, *J. Electroanal. Chem.* **2000**, *489*, 55.
[46] T. Ohzuku, Y. Iwakoshi, K. Sawai, *J. Electrochem. Soc.* **1993**, *140*, 2490.
[47] Z. Wang, S. M. Selbach, T. Grande, *RSC Adv.* **2014**, *4*, 4069.
[48] T. Zheng, Y. Liu, E. W. Fuller, S. Tseng, U. Sacken, J. R. Dahn, *J. Electrochem. Soc.* **1995**, *142*, 2581.
[49] D. Aurbach, Y. Gofer, J. Langzam, *J. Electrochem. Soc.* **1989**, *136*, 3198.
[50] J. Purewal, *PhD. Degree Thesis*, California Institute of Technology, Pasadena, CA **2010**.
[51] R. Tossici, M. Berrettoni, V. Nalimova, R. Marassi, B. Scrosati, *J. Electrochem. Soc.* **1996**, *143*, L64.
[52] H. Kim, J. Hong, Y. Park, J. Kim, I. Hwang, K. Kang, *Adv. Funct. Mater.* **2015**, *25*, 534.
[53] A. Ponrouch, E. Marchante, M. Courty, J. M. Tarascon, M. R. Palacín, *Energy Environ. Sci.* **2012**, *5*, 8572.
[54] A. Ponrouch, R. Dedryvere, D. Monti, J. M. Ateba Mba, L. Croguennec, C. Masquelier, P. Johansson, M. R. Palacín, *Energy Environ. Sci.* **2013**, *6*, 2361.
[55] M. Dahbi, N. Yabuuchi, K. Kubota, K. Tokiwa, S. Komaba, *Phys. Chem. Chem. Phys.* **2014**, *16*, 15007.
[56] A. Funabiki, M. Inaba, T. Abe, Z. Ogumi, *J. Electrochem. Soc.* **1999**, *146*, 2443.
[57] C. Wang, A. J. Appleby, F. E. Little, *J. Electroananl. Chem.* **2001**, *497*, 33.